Existence of interfacial polaronic plasmon: A comparative study between FeSe/$SrTiO_3$ and CoSe/$SrTiO_3$

Xiaofeng Xu,[1,2] Shuyuan Zhang,[3] Jiaqi Guan,[4] Jiade Li,[1,2] Guangyao Miao,[1,2] Zhiyu Tao,[1,2] Weihua Wang,[1,5] Xuetao Zhu,[1,2,5,*] and Jiandong Guo[1,2,5,†]

[1]*Beijing National Laboratory for Condensed Matter Physics and Institute of Physics, Chinese Academy of Sciences, Beijing 100190, China*
[2]*School of Physical Sciences, University of Chinese Academy of Sciences, Beijing 100049, China*
[3]*Department of Physics, Laboratory of Atomic and Solid State Physics, Cornell University, Ithaca, New York 14853, USA*
[4]*Instrumentation and Service Center for Physical Sciences, Westlake University, Hangzhou 310024, Zhejiang, China*
[5]*Songshan Lake Materials Laboratory, Dongguan, Guangdong 523808, China*

(Received 13 January 2022; revised 2 March 2022; accepted 2 March 2022; published 14 March 2022)

The discovery of monolayer FeSe on $SrTiO_3$ (STO) with the boosting superconducting transition temperature has prompted an intense increase in experimental and theoretical researches on interfacial superconductivity enhancement. One of the most concerning research subjects is to explore the nature of the interfacial coupling. Here, we performed a comparative study between the isostructural CoSe/STO and FeSe/STO by measuring the phonons and plasmons via high-resolution electron energy loss spectroscopy. With the increasing thickness of the epitaxial film, the measured intensity of the Fuchs-Kliewer (F-K) phonons and the plasmon from STO decay much faster in the CoSe film than those in FeSe, owing to the higher carrier concentration in CoSe. By comparing the temperature-dependent behaviors of the F-K phonons and plasmons, we discovered that the interfacial coupling in CoSe/STO is adiabatic because of its large Fermi energy. In contrast, the interfacial electron-phonon coupling in FeSe/STO is nonadiabatic, resulting in the formation of interfacial polarons that plays an important role in the superconductivity enhancement.

DOI: 10.1103/PhysRevB.105.125410

I. INTRODUCTION

Single-layer FeSe film grown on $SrTiO_3$ (1 uc-FeSe/STO) [1] has been receiving growing attention due to the characteristics of simple structure and high superconducting temperature [2–10]. The superconducting gap opening temperature T_g of 1 uc-FeSe/STO reaches up to 60–70 K [11–13], which is almost one order of magnitude higher than the superconducting transition temperature $T_c \sim 8$ K [14] of the pristine FeSe at ambient pressure. Although electron doping [15–23] and interfacial coupling [1,24–32] are widely regarded as two essential factors for the substantially enhanced superconductivity in FeSe/STO, the inherent physical picture of the enhancement mechanism remains elusive at present and deserves further efforts to explore.

The enhancement mechanism in most of the existing studies has pointed to the electron-phonon coupling (EPC) across the interface [24,29,33,34]. The model of dynamic interfacial polaron [33] is a representative picture in which the EPC between FeSe and oxide substrates is interpreted from the perspective of elementary excitations. In the dynamic interfacial polaron model, the Fuchs-Kliewer (F-K) phonons [35] widely existing in the oxide substrates play a key role: The F-K phonons accompanied with a dipole field can penetrate into the FeSe films [28,30] and dress electrons therein, forming the interfacial polarons [33]. Most importantly, a proper electron density positions 1 uc-FeSe/STO into the framework of nonadiabatic EPC where the Fermi energy (E_F) is lower than the phonon energy ($\hbar\omega$). The nonadiabatic EPC has been theoretically proved to give rise to a strong enhancement of T_c with respect to the usual theory (Migdal's theorem) within the framework of adiabatic EPC [36–38]. In contrast to the adiabatic EPC in metals ($E_F \gg \hbar\omega$) where the response of phonons to the fast electrons are retarded, in the nonadiabatic model ($E_F \leqslant \hbar\omega$) phonons respond instantly to the slowly moving electrons so that interfacial polarons can move in the lattice. These dynamic polarons are proposed to yield the strengthened Cooper pairing, which may be responsible for the dramatically boosted superconductivity in FeSe/STO.

Despite these appealing progress, the condition of the nonadiabatic interfacial EPC is still not experimentally confirmed. Especially, why the nonadiabatic interfacial coupling only occurs in FeSe/STO needs to be experimentally explored.

In this context, CoSe film grown on STO with considerably larger E_F [40,42] than FeSe stands out as a strong candidate. In this paper, using high-resolution electron energy loss spectroscopy (HREELS), we present an extensive comparative study of the phonons and plasmons in the isostructural FeSe/STO and CoSe/STO. The phonon branches in FeSe and CoSe films, F-K phonons from STO, as well as the polaronic plasmons across the interfaces, were unambiguously revealed in the HREELS spectra of both FeSe/STO and CoSe/STO.

*xtzhu@iphy.ac.cn
†jdguo@iphy.ac.cn

It is found that both the F-K phonons and the plasmon are more strongly screened by CoSe compared to FeSe due to the much higher carrier density in CoSe films. More importantly, in striking contrast to FeSe/STO where the F-K phonons and the plasmon decay synchronously with temperature increasing, they exhibit a nonsynchronous decay behavior in CoSe/STO. This indicates the absence of interfacial polarons in CoSe/STO as a result of the adiabatic nature of EPC therein. Our results demonstrate that the proper band structure and Fermi level in FeSe happen to well satisfy the nonadiabatic EPC condition, which is an essential factor for the significantly enhanced T_c in FeSe/STO.

II. METHODS

Before the epitaxial growth of FeSe and CoSe films, the Nb-doped (0.5 wt %) STO (001) substrates were pretreated in ultrahigh vacuum at 1000 °C for 1 h to obtain a TiO_2-terminated surface. The FeSe films were grown on STO by molecular beam epitaxy (MBE), the details of the growth can be found in previous studies [1,30]. CoSe films with different thicknesses were grown by co-depositing high-purity Co (99.995%) and Se (99.999%) from Knudsen cells with a flux ratio of 1:5 onto the treated STO held at 360 °C [40,42]. All the samples were characterized by scanning tunneling microscopy (STM) to confirm the high quality.

To prevent surface contamination, the FeSe/STO samples were capped with amorphous Se layer and then transferred into the HREELS system followed by *in situ* annealing at 450 °C for 3 h to make the first layer of FeSe superconducting. And T_g of 1 uc-FeSe/STO is around 65 K, determined by *in situ* angle-resolved photoemission spectroscopy (ARPES) [30]. The CoSe/STO samples were transferred from MBE to HREELS via a homemade vacuum suitcase with a base pressure better than 1×10^{-9} Torr. Low-energy electron diffraction (LEED) patterns were taken at 300 K to further verify the sample quality and determine the crystallographic direction. The HREELS measurements were carried out on a system with the capability of two-dimensional (2D) energy-momentum mapping [43]. The used incident electron-beam energies were $E_i = 50$ and 110 eV and the scattering direction was along the $\bar{\Gamma}$-$\bar{X}$ direction for both FeSe and CoSe samples if not specified otherwise. The incident angle used in the measurements was 60° with respect to the surface normal. The energy resolution was about 3 meV.

The phonon dispersion of CoSe was calculated using the PHONOPY code through the density functional perturbation theory method [44] on a $4 \times 4 \times 1$ supercell. Here, the Hubbard U correction via the Perdew-Burke-Ernzerhof (PBE) + U method [45] was applied for considering the correlation effect associated with the Co-3d orbitals. The forces were calculated with the Vienna *ab initio* simulation package code. The generalized gradient approximation of PBE [46,47] was used for the exchange-correlation potential. The plane-wave energy cutoff was set to be 400 eV. All the structures were adequately optimized with the energy and force convergence criteria of 10^{-7} eV and 10^{-4} eV/Å, respectively. The calculation of the phonon dispersion of FeSe was adopted from our previous study [30].

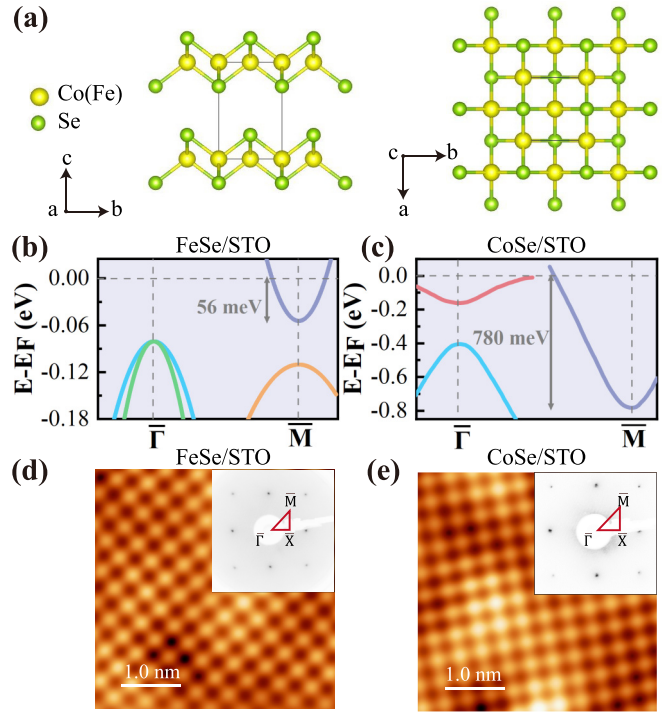

FIG. 1. (a) Top and side views of the atomic structure of anti-PbO-type CoSe (FeSe). (b) and (c) Schematics of the electronic band structure along $\bar{\Gamma}$-$\bar{M}$ of 1 uc-FeSe/STO and 1 uc-CoSe/STO, respectively, extracted from Refs. [39,40]. The double-headed arrows indicate the value of the Fermi energy. (d) and (e) Atomically resolved STM images (obtained by WSXM [41]) of 1 uc-FeSe/STO and 1 uc-CoSe/STO measured at 4.8 K, respectively. The insets in (d) and (e) are the corresponding LEED patterns taken at 300 K with the primary energy of 80 and 65 eV, respectively. Red lines represent the least irreducible surface Brillouin zone.

III. RESULTS AND DISCUSSION

A. Crystal and band structure

As schematically depicted in Fig. 1(a), anti-PbO-type CoSe shares a similar crystal structure with FeSe, consisting of Se-Co-Se triple layers stacked by van der Waals interactions along the c axis [40,42,48–50]. Furthermore, the band structure of monolayer CoSe on STO resembles that of its iron analog, except for the chemical potential remarkably shifted up as a result of the fact that Co atom donates one more electron from the 3d shell than the Fe atom [40,42]. For clarity, the band structure of 1 uc-FeSe/STO and 1 uc-CoSe/STO along the $\bar{\Gamma}$-$\bar{M}$ direction extracted from Refs. [33,39,40] are presented in Figs. 1(b) and 1(c) where the E_F of CoSe is about 780 meV, much higher than 56 meV in FeSe. Thus, there is a great difference in the electron density between CoSe and FeSe, which is consistent with the results by the transport measurements [40,51] and ARPES [42,52]. The LEED patterns of 1 uc-FeSe/STO and 1 uc-CoSe/STO [insets of Figs. 1(d) and 1(e)] captured at 300 K both show sharp diffraction spots. Additionally, the corresponding atomic-resolution images from STM measured at 4.8 K [Figs. 1(d) and 1(e), respectively] reveal well-defined tetragonal lattices. All the results here indicate the high quality of our

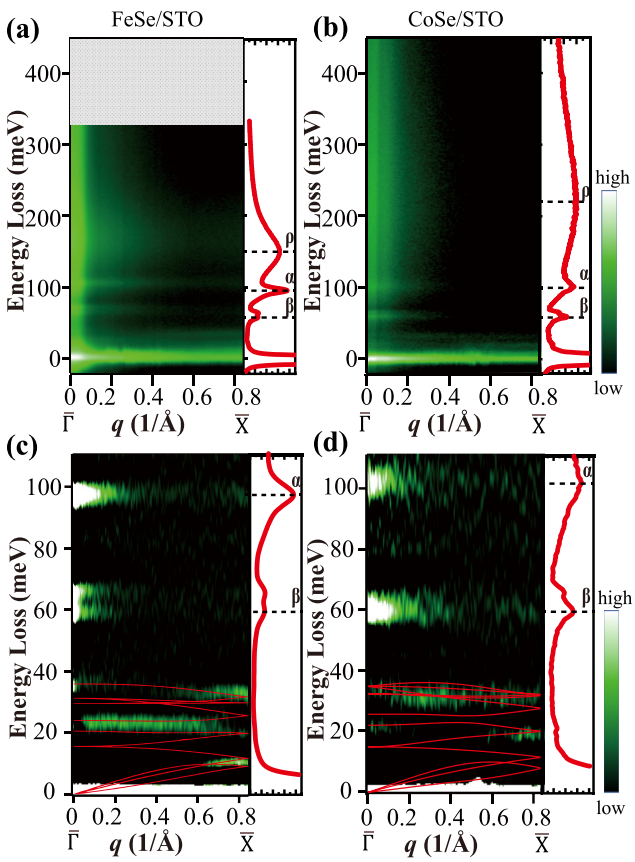

FIG. 2. (a) and (b) Energy-momentum mapping of 2D-HREELS measurements along the $\bar{\Gamma}$-$\bar{X}$ direction at 35 K of 1 uc-FeSe/STO and 1 uc-CoSe/STO, respectively. (c) and (d) Second derivative images of (a) and (b) from 0 to 110 meV, superimposed with the calculated phonon spectra of FeSe and CoSe films, respectively. The right panel of each figure shows the corresponding energy distribution curve (EDC) at $q = 0$.

samples and guarantee the reliability of data obtained via HREELS.

B. Two-dimensional-HREELS measurements

The HREELS measurements reveal the energy-loss signals from FeSe and CoSe films on STO. Figures 2(a) and 2(b) show the energy and momentum mapping of 1 uc-FeSe/STO and 1 uc-CoSe/STO, respectively, taken at 35 K along the $\bar{\Gamma}$-$\bar{X}$ direction. As exhibited in the energy distribution curves (EDCs) at $q = 0$ [the right panels of Figs. 2(a) and 2(b)], three apparent energy-loss modes labeled by α, β, and ρ can be discerned in both samples. α ($\sim$100 meV) and β ($\sim$60 meV) in 1 uc-CoSe/STO are identified as the F-K surface phonons in the STO substrate [28,53], demonstrating that the electric field induced by the F-K phonons can also penetrate into a monolayer CoSe film and be detected in HREELS, the same as that in FeSe/STO. Another branch ρ ($\sim$220 meV) with relatively high energy is recognized as the polaronic plasmon [54], which will be discussed in detail in the following. In addition, Figs. 2(c) and 2(d) show the second derivative images of Figs. 2(a) and 2(b) in the energy region from 0 to 110 meV, respectively. Besides the F-K phonon modes (α and β) from the STO substrate, the phonon branches of CoSe and FeSe films are clearly observed within the energy range of 0–40 meV. These phonon modes can also be discerned in the calculated phonon dispersions of FeSe and CoSe films denoted as the red solid lines superimposed on the images. It is worth noting that only those phonon modes following the selection rule of the impacting scattering [55,56] can be detected in the HREELS measurements, and, thus, not all the calculated branches have a one-to-one correspondence in the experimental results here. In this paper, we mainly discuss the features of the STO F-K phonons (α and β) as well as the plasmon mode ρ in FeSe/STO and CoSe/STO.

C. Temperature-dependent HREELS

To gain more insights into the plasmon and the F-K phonons after different films grown on STO, we performed temperature-dependent HREELS measurements from 35 to 300 K. Figure 3 displays the stacked EDCs at the $\bar{\Gamma}$ point at several temperatures for the treated STO, 1 uc-FeSe/STO and 1 uc-CoSe/STO. In all three samples, the F-K phonons α and β show no obvious change, whereas the energy of plasmon ρ decreases dramatically with temperature increasing. In conventional doped semiconductors, the plasmon energy usually increases due to the thermal excitations of carriers upon temperature increase [57]. The anomalous behavior of the plasmon observed here has been proved to relate to the polar semiconductor nature of doped STO in which the electrons and their companying lattice polarization (or phonons) form quasiparticles called polarons [58]. The anomalous temperature dependence was attributed to an increase in the effective mass of the polarons that give rise to the plasmon mode therein [59–61]. And the plasmon mode resulting from the collective excitation of polarons was called the polaronic plasmon [54]. Consequently, we infer that the plasmon modes observed in 1 uc-FeSe/STO and 1 uc-CoSe/STO are also polaronic plasmons.

Although they show similar anomalous temperature-dependent behavior, the energy of the polaronic plasmon varies a lot in these samples at low temperature: 223 meV for CoSe/STO, 152 meV for FeSe/STO and 186 meV for STO, seen in Fig. 4. Taking STO as a reference, a blueshift is clearly observed in CoSe/STO, whereas a redshift is observed in FeSe/STO. The reverse shift can be attributed to the difference in charge transfer between the film and the STO substrate, which is consistent with the reported STM results [40]. From the Fermi level shown in Figs. 1(b) and 1(c), there is a great disparity of carrier density in CoSe and FeSe. The density of electrons in the CoSe film is much higher than that of the STO substrate, and, thus, electrons should move from CoSe towards STO, either accumulate at the interface or transfer into the STO substrate. In contrast, the density of electrons in the FeSe film is lower than the STO substrate so that electrons transfer from STO into the FeSe film [16,62,63].

D. Decay of the F-K phonon and the plasmon

Aside from the electron transfer across the interface, the coupling between the film and the substrate is another focus

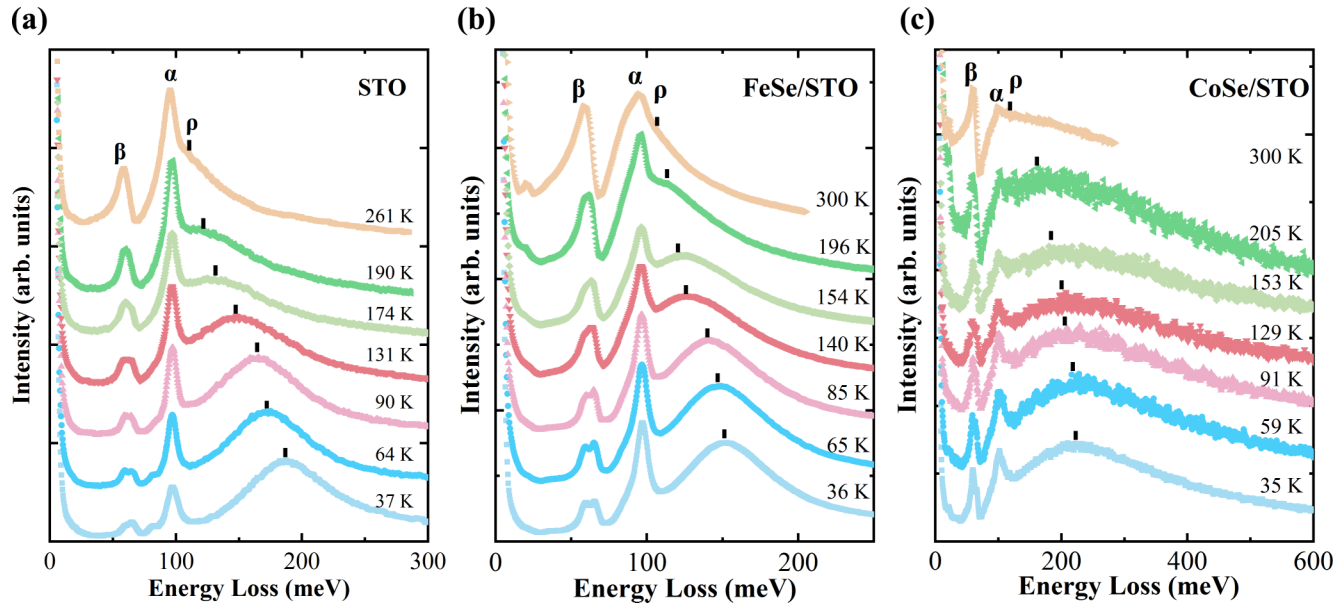

FIG. 3. Comparison of the EDCs at the $\bar{\Gamma}$ point with varying temperature in (a) STO, (b) 1uc-FeSe/STO, and (c) 1 uc-CoSe/STO, respectively.

in this paper. We performed the HREELS measurements on samples with various CoSe (FeSe) film thicknesses in order to study the interaction of the CoSe (FeSe) film and the STO substrate. Figures 5(a) and 5(b) exhibit the stacked EDCs at the $\bar{\Gamma}$ point for FeSe and CoSe samples, respectively, with different film thicknesses. With film thickness increasing, the intensities of the F-K phonons (α and β) and the polaronic plasmon (ρ) all show an obvious decay in both FeSe/STO and CoSe/STO. The intensity of the HREELS spectrum is not only related to the intrinsic sample properties, but also to the extrinsic instrument effect. Here, with all experimental conditions maintained, but only the film thickness changed, it allows us to quantitatively determine the intensity decay length. After subtracting the background mainly involving the extrinsic effect, we extract the normalized intensity of the phonon mode α and the plasmon ρ from Figs. 5(a) and 5(b) with the results plotted in Fig. 5(c). By fitting the intensity with an exponential curve (solid lines), it is found that the decay lengths of α and ρ in CoSe/STO are both 1.0 uc, significantly shorter than the value of 2.5 uc (α) and 3.8 uc (ρ) in FeSe/STO, suggesting the electric fields induced by the F-K phonons and the plasmon are almost fully screened by the large density of electrons existing in CoSe.

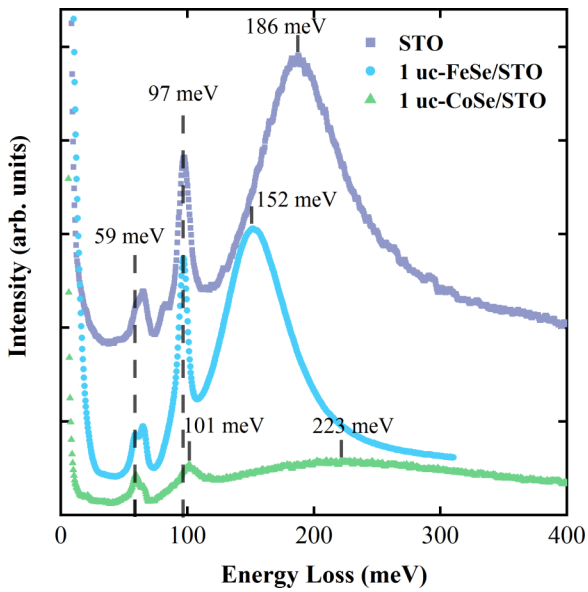

FIG. 4. EDCs at the $\bar{\Gamma}$ point for STO, 1 uc-FeSe/STO, and 1 uc-CoSe/STO at low temperature (35–37 K) with $E_i = 110$ eV. The dashed lines are guides to the eye.

Additionally, a redshift of plasmon as the thickness increases in FeSe/STO is also shown in Fig. 5(a). It is worth noting that both the EPC and the carrier density will influence the energy of the polaronic plasmon. Although there is charge transfer from STO into FeSe which could decrease the energy of plasmon, the electrons are proved to only accumulate within the first two layers of the FeSe films near STO [23]. Consequently, such a continuous redshift with increasing film thickness can be mainly attributed to the EPC which attenuates with increasing thickness. In contrast, a blueshift is observed in CoSe/STO [Fig. 5(b)] as a result of the considerable electron transfer from CoSe towards the STO interface rather than the coupling effect.

E. Adiabatic or nonadiabatic interfacial coupling?

To further find out the particularity from the perspective of elementary excitations in FeSe/STO, we extract the energy of the polaronic plasmon ρ and the F-K phonon α upon varying the temperature from Fig. 3 with the results illustrated in Fig. 6. For FeSe/STO, the temperature dependence of the F-K phonon is astonishingly synchronous to that of the polaronic plasmon as shown in Fig. 6(b). The synchronous behavior indicates that the F-K phonons in STO participate

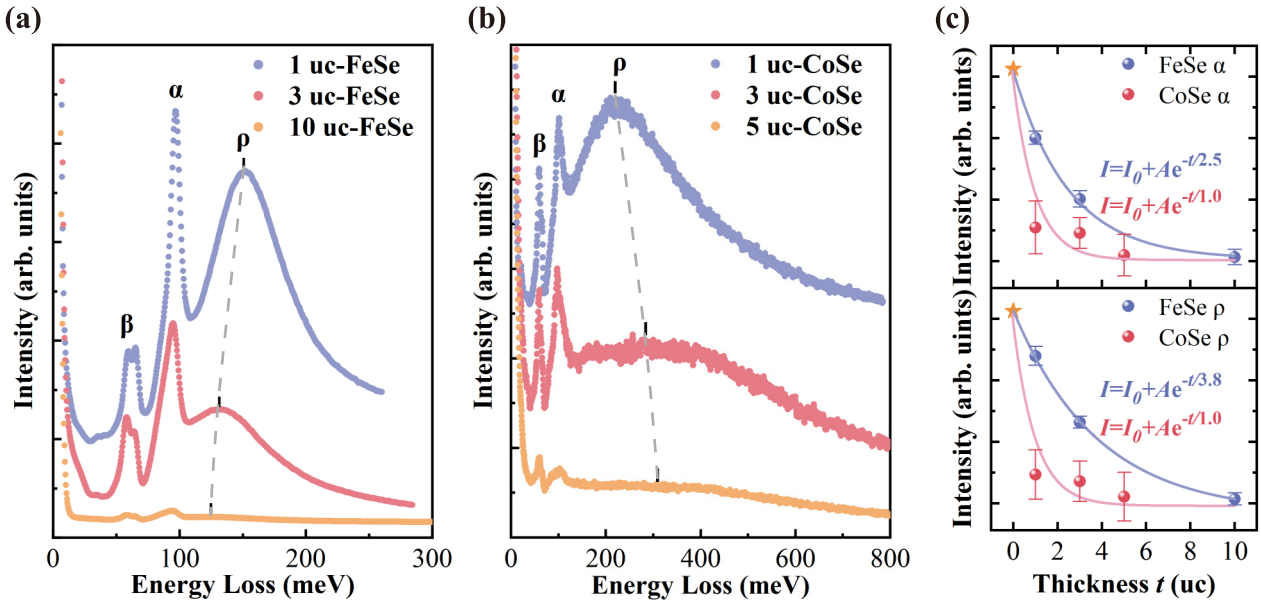

FIG. 5. (a) and (b) Comparison of the EDCs with different thicknesses at the $\bar{\Gamma}$ point at 35 K for FeSe/STO and CoSe/STO, respectively. The dashed lines indicate the trend of energy shift of the plasmon as guides to the eye. (c) Plot and exponential fitting of the intensity of the F-K phonon α (upper panel) and the plasmon ρ (lower panel) as a function of the film thickness for FeSe and CoSe. The yellow star denotes the intensity of bare STO. Here, the intensity of the phonon and plasmon of FeSe/STO (CoSe/STO) is normalized by that of bare STO with $E_i = 50$ eV (110 eV). The error bars are from different background subtraction methods used in the peak fitting.

in the formation of the interfacial polaronic plasmon [33]. The electrons in the FeSe film are part of the interfacial polarons. Consequently, such an interface-related plasmon gives rise to a longer decay length compared with the F-K phonon [Fig. 5(c)]. However, CoSe/STO shows similar behaviors with STO, i.e., the plasmon is strongly temperature dependent, whereas the F-K phonon is weakly temperature dependent [Figs. 6(a) and 6(c)]. The independent decay behavior in CoSe/STO hints that the F-K phonon does not participate in the formation of the polaronic plasmon. This feature explicitly demonstrates that the polaronic plasmon of CoSe/STO totally originates from polarons in STO, consistent with the view of electron transfer from CoSe into the substrate. So it is reasonable that the decay length of plasmon and the F-K phonon is the same in CoSe/STO [Fig. 5(c)] since both of them are related to the dipole field from the STO that penetrates the CoSe films. This fact, hence, provides more specific evidence of the strong interaction between the F-K phonons in STO

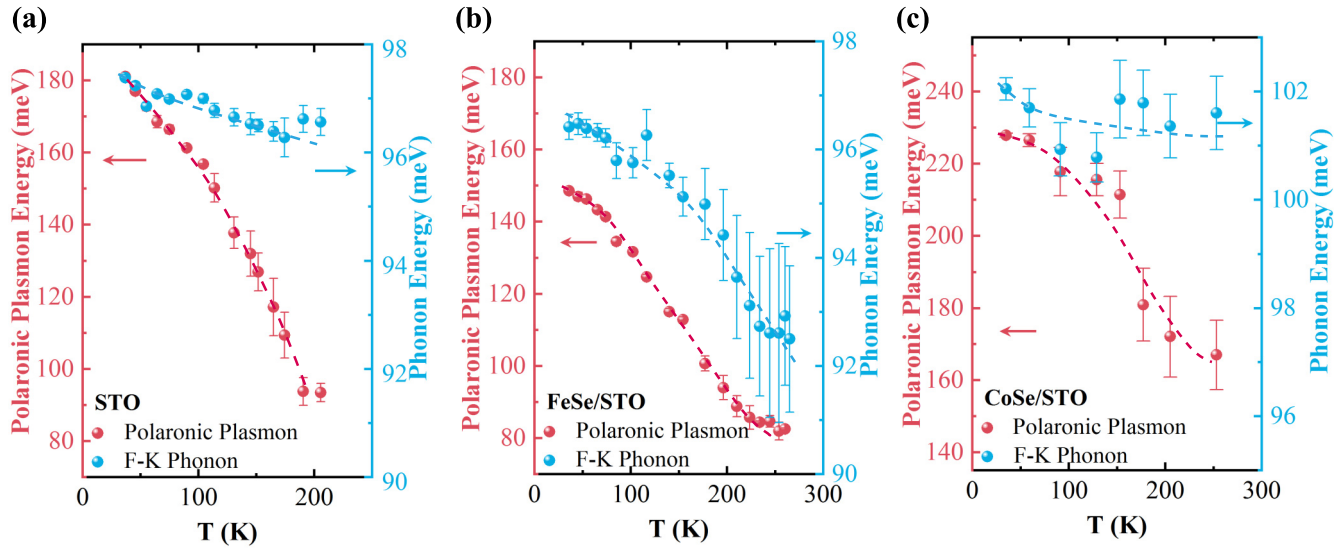

FIG. 6. Comparison of the energies of the polaronic plasmon ρ and the F-K phonon α at different temperatures extracted from Fig. 3 for (a) STO, (b) FeSe/STO, and (c) CoSe/STO, respectively. The dashed lines are guides to the eye. The error bars are from different background subtraction methods used in the peak fitting.

with the electrons in FeSe film and consolidates the existence of interfacial polarons [33].

As previously reported, the nonadiabatic EPC is the key to forming the interfacial polarons [33]. The different polaron nature between FeSe/STO and CoSe/STO is largely attributed to the distinct Fermi energies as illustrated in Figs. 1(b) and 1(c). For 1 uc-FeSe/STO, the E_F (56 meV) is much smaller than the energy of the F-K phonon α (97 meV), leading the EPC to be nonadiabatic. On the contrary, for 1 uc-CoSe/STO, the E_F (780 meV) is far larger than the energy of the α mode (97 meV), going beyond the framework of nonadiabatic EPC. Even if there was EPC in the CoSe films, it would be the adiabatic EPC, such as the cases in metals in which the electrons move much more quickly than the phonons. Since the Fermi energy plays an important role in the nature of the EPC, it would be helpful to investigate the relationship between the EPC and superconductivity by tuning the Fermi level in one system, e.g., Co-doped FeSe/STO. Base on FeSe/STO samples with a superconducting gap of 16 meV, previous STM measurements demonstrated that the substitution of Fe with Co indeed provides extra electrons and shifts up the Fermi level [64]. The superconductivity is substantially suppressed within the doping area, pointing to the adiabatic EPC. Therefore, the above analyses generate two clear results: (1) the interfacial polarons can hardly form when the E_F of the system is larger than the phonon energy of STO; and (2) the nonadiabatic EPC present in FeSe/STO is not a coincidence but an indispensable factor for the superconductivity enhancement.

IV. CONCLUSIONS

The comparison of the HREELS spectra between CoSe/STO and FeSe/STO demonstrates that the penetration of the F-K phonons and plasmon into the film is more strongly screened due to the larger electron density in CoSe films. Moreover, the nonsynchronous decay behavior as well as the same screening length of the F-K phonons and the plasmon in CoSe/STO evidence the failure of the formation of interfacial polarons. This is attributed to the fact that the condition of the nonadiabatic interfacial coupling is not satisfied in CoSe/STO since the Fermi energy in CoSe is much larger than the highest phonon energy of STO. In contrast, the behaviors of the phonons and the plasmon in FeSe/STO consolidate the existence of the nonadiabatic interfacial coupling. The current comparative HREELS study further verifies the essential role of the nonadiabatic EPC in FeSe/STO, which may become a new barometer for the exploration of more systems with pronounced interfacial superconductivity enhancement.

ACKNOWLEDGMENTS

This work was supported by the National Key R&D Program of China (Grants No. 2017YFA0303600 and No. 2021YFA1400200), the National Natural Science Foundation of China (Grants No. 11874404, No. 11974399, and No. 11974402), and the Strategic Priority Research Program of Chinese Academy of Sciences (Grant No. XDB33000000). X.Z. was partially supported by the Youth Innovation Promotion Association of Chinese Academy of Sciences.

[1] Q.-Y. Wang, Z. Li, W.-H. Zhang, Z.-C. Zhang, J.-S. Zhang, W. Li, H. Ding, Y.-B. Ou, P. Deng, K. Chang, J. Wen, C.-L. Song, K. He, J.-F. Jia, S.-H. Ji, Y.-Y. Wang, L.-L. Wang, X. Chen, X.-C. Ma, and Q.-K. Xue, Chin. Phys. Lett. **29**, 037402 (2012).

[2] L. Wang, X. Ma, and Q.-K. Xue, Supercond. Sci. Technol. **29**, 123001 (2016).

[3] I. Nekrasov, N. Pavlov, M. Sadovskii, and A. Slobodchikov, Low Temp. Phys. **42**, 891 (2016).

[4] M. V. Sadovskii, Phys.-Usp. **59**, 947 (2016).

[5] Z. Wang, C. Liu, Y. Liu, and J. Wang, J. Phys.: Condens. Matter **29**, 153001 (2017).

[6] A. Kreisel, P. J. Hirschfeld, and B. M. Andersen, Symmetry **12**, 1402 (2020).

[7] D. Huang and J. E. Hoffman, Annu. Rev. Condens. Matter Phys. **8**, 311 (2017).

[8] D.-H. Lee, Annu. Rev. Condens. Matter Phys. **9**, 261 (2018).

[9] C. Liu and J. Wang, 2D Mater. **7**, 022006 (2020).

[10] X. Xu, S. Zhang, X. Zhu, and J. Guo, J. Phys.: Condens. Matter **32**, 343003 (2020).

[11] S. Tan, Y. Zhang, M. Xia, Z. Ye, F. Chen, X. Xie, R. Peng, D. Xu, Q. Fan, H. Xu *et al.*, Nature Mater. **12**, 634 (2013).

[12] S. He, J. He, W. Zhang, L. Zhao, D. Liu, X. Liu, D. Mou, Y.-B. Ou, Q.-Y. Wang, Z. Li *et al.*, Nat. Mater. **12**, 605 (2013).

[13] W. Zhang, Y. Sun, J.-S. Zhang, F.-S. Li, M.-H. Guo, Y.-F. Zhao, H.-M. Zhang, J.-P. Peng, Y. Xing, H.-C. Wang *et al.*, Chin. Phys. Lett. **31**, 017401 (2014).

[14] F.-C. Hsu, J.-Y. Luo, K.-W. Yeh, T.-K. Chen, T.-W. Huang, P. M. Wu, Y.-C. Lee, Y.-L. Huang, Y.-Y. Chu *et al.*, Proc. Natl. Acad. Sci. U.S.A. **105**, 14262 (2008).

[15] Z. Li, J.-P. Peng, H.-M. Zhang, W.-H. Zhang, H. Ding, P. Deng, K. Chang, C.-L. Song, S.-H. Ji, L. Wang *et al.*, J. Phys.: Condens. Matter **26**, 265002 (2014).

[16] W. Zhang, Z. Li, F. Li, H. Zhang, J. Peng, C. Tang, Q. Wang, K. He, X. Chen, L. Wang, X. Ma, and Q.-K. Xue, Phys. Rev. B **89**, 060506(R) (2014).

[17] Y. Miyata, K. Nakayama, K. Sugawara, T. Sato, and T. Takahashi, Nat. Mater. **14**, 775 (2015).

[18] C. Tang, D. Zhang, Y. Zang, C. Liu, G. Zhou, Z. Li, C. Zheng, X. Hu, C. Song, S. Ji, K. He, X. Chen, L. Wang, X. Ma, and Q.-K. Xue, Phys. Rev. B **92**, 180507(R) (2015).

[19] J. Shiogai, Y. Ito, T. Mitsuhashi, T. Nojima, and A. Tsukazaki, Nat. Phys. **12**, 42 (2016).

[20] C.-L. Song, H.-M. Zhang, Y. Zhong, X.-P. Hu, S.-H. Ji, L. Wang, K. He, X.-C. Ma, and Q.-K. Xue, Phys. Rev. Lett. **116**, 157001 (2016).

[21] W. Zhang, X. Liu, C. Wen, R. Peng, S. Tan, B. Xie, T. Zhang, and D. Feng, Nano Lett. **16**, 1969 (2016).

[22] J. Guan, J. Liu, B. Liu, X. Huang, Q. Zhu, X. Zhu, J. Sun, S. Meng, W. Wang, and J. Guo, Phys. Rev. B **95**, 205405 (2017).

[23] W. Zhao, M. Li, C.-Z. Chang, J. Jiang, L. Wu, C. Liu, J. S. Moodera, Y. Zhu, and M. H. Chan, Sci. Adv. **4**, eaao2682 (2018).

[24] J. Lee, F. Schmitt, R. Moore, S. Johnston, Y.-T. Cui, W. Li, M. Yi, Z. Liu, M. Hashimoto, Y. Zhang *et al.*, Nature (London) **515**, 245 (2014).

[25] Y.-T. Cui, R. G. Moore, A.-M. Zhang, Y. Tian, J. J. Lee, F. T. Schmitt, W.-H. Zhang, W. Li, M. Yi, Z.-K. Liu, M. Hashimoto, Y. Zhang, D.-H. Lu, T. P. Devereaux, L.-L. Wang, X.-C. Ma, Q.-M. Zhang, Q.-K. Xue, D.-H. Lee, and Z.-X. Shen, Phys. Rev. Lett. **114**, 037002 (2015).

[26] D.-H. Lee, Chin. Phys. B **24**, 117405 (2015).

[27] C. Tang, C. Liu, G. Zhou, F. Li, H. Ding, Z. Li, D. Zhang, Z. Li, C. Song, S. Ji, K. He, L. Wang, X. Ma, and Q.-K. Xue, Phys. Rev. B **93**, 020507(R) (2016).

[28] S. Zhang, J. Guan, X. Jia, B. Liu, W. Wang, F. Li, L. Wang, X. Ma, Q. Xue, J. Zhang, E. W. Plummer, X. Zhu, and J. Guo, Phys. Rev. B **94**, 081116(R) (2016).

[29] Y. C. Tian, W. H. Zhang, F. S. Li, Y. L. Wu, Q. Wu, F. Sun, G. Y. Zhou, L. Wang, X. Ma, Q.-K. Xue, and J. Zhao, Phys. Rev. Lett. **116**, 107001 (2016).

[30] S. Zhang, J. Guan, Y. Wang, T. Berlijn, S. Johnston, X. Jia, B. Liu, Q. Zhu, Q. An, S. Xue, Y. Cao, F. Yang, W. Wang, J. Zhang, E. W. Plummer, X. Zhu, and J. Guo, Phys. Rev. B **97**, 035408 (2018).

[31] N. Andrejevic, F. Han, T. Nguyen, A. Puretzky, Q. Meng, Y.-F. Zhao, W. Zhao, L. Wu, D. Geohegan, C.-Z. Chang, Y. Zhu, S. Huang, and M. Li, arXiv:1908.05648.

[32] B. D. Faeth, S. Xie, S. Yang, J. K. Kawasaki, J. N. Nelson, S. Zhang, C. Parzyck, P. Mishra, C. Li, C. Jozwiak, A. Bostwick, E. Rotenberg, D. G. Schlom, and K. M. Shen, Phys. Rev. Lett. **127**, 016803 (2021).

[33] S. Zhang, T. Wei, J. Guan, Q. Zhu, W. Qin, W. Wang, J. Zhang, E. W. Plummer, X. Zhu, Z. Zhang, and J. Guo, Phys. Rev. Lett. **122**, 066802 (2019).

[34] Q. Song, T. Yu, X. Lou, B. Xie, H. Xu, C. Wen, Q. Yao, S. Zhang, X. Zhu, J. Guo *et al.*, Nat. Commun. **10**, 758 (2019).

[35] R. Fuchs and K. Kliewer, Phys. Rev. **140**, A2076 (1965).

[36] C. Grimaldi, L. Pietronero, and S. Strässler, Phys. Rev. Lett. **75**, 1158 (1995).

[37] L. Pietronero, S. Strässler, and C. Grimaldi, Phys. Rev. B **52**, 10516 (1995).

[38] C. Grimaldi, L. Pietronero, and S. Strässler, Phys. Rev. B **52**, 10530 (1995).

[39] D. Huang, C.-L. Song, T. A. Webb, S. Fang, C.-Z. Chang, J. S. Moodera, E. Kaxiras, and J. E. Hoffman, Phys. Rev. Lett. **115**, 017002 (2015).

[40] C. Liu, F. Zheng, L. Shen, M. Liao, R. Wu, G. Gong, C. Ding, H. Yang, W. Li, C.-L. Song *et al.*, Supercond. Sci. Technol. **31**, 115011 (2018).

[41] I. Horcas, R. Fernández, J. Gomez-Rodriguez, J. Colchero, J. Gómez-Herrero, and A. Baro, Rev. Sci. Instrum. **78**, 013705 (2007).

[42] L. Shen, C. Liu, F. W. Zheng, X. Xu, Y. J. Chen, S. C. Sun, L. Kang, Z. K. Liu, Q. K. Xue, L. L. Wang, Y. L. Chen, and L. X. Yang, Phys. Rev. Mater. **2**, 114005 (2018).

[43] X. Zhu, Y. Cao, S. Zhang, X. Jia, Q. Guo, F. Yang, L. Zhu, J. Zhang, E. Plummer, and J. Guo, Rev. Sci. Instrum. **86**, 083902 (2015).

[44] S. Baroni, S. De Gironcoli, A. Dal Corso, and P. Giannozzi, Rev. Mod. Phys. **73**, 515 (2001).

[45] S. L. Dudarev, G. A. Botton, S. Y. Savrasov, C. J. Humphreys, and A. P. Sutton, Phys. Rev. B **57**, 1505 (1998).

[46] J. P. Perdew, J. A. Chevary, S. H. Vosko, K. A. Jackson, M. R. Pederson, D. J. Singh, and C. Fiolhais, Phys. Rev. B **46**, 6671 (1992).

[47] P. E. Blöchl, Phys. Rev. B **50**, 17953 (1994).

[48] X. Zhou, B. Wilfong, H. Vivanco, J. Paglione, C. M. Brown, and E. E. Rodriguez, J. Am. Chem. Soc. **138**, 16432 (2016).

[49] B. Wilfong, X. Zhou, H. Vivanco, D. J. Campbell, K. Wang, D. Graf, J. Paglione, and E. Rodriguez, Phys. Rev. B **97**, 104408 (2018).

[50] B. Tai, W. Wu, X. Feng, Y. Jiao, J. Zhao, Y. Lu, X.-L. Sheng, and S. A. Yang, Phys. Rev. B **102**, 224422 (2020).

[51] Y. Sun, W. Zhang, Y. Xing, F. Li, Y. Zhao, Z. Xia, L. Wang, X. Ma, Q.-K. Xue, and J. Wang, Sci. Rep. **4**, 6040 (2014).

[52] D. Liu, W. Zhang, D. Mou, J. He, Y.-B. Ou, Q.-Y. Wang, Z. Li, L. Wang, L. Zhao, S. He *et al.*, Nat. Commun. **3**, 931 (2012).

[53] H. Vogt, Phys. Rev. B **38**, 5699 (1988).

[54] A. S. Alexandrov and N. F. Mott, *Polarons and Bipolarons* (World Scientific, Singapore, 1996).

[55] H. Ibach and D. L. Mills, *Electron Energy Loss Spectroscopy and Surface Vibrations* (Academic press, New York, 2013).

[56] F. de Juan, A. Politano, G. Chiarello, and H. A. Fertig, Carbon **85**, 225 (2015).

[57] E. T. Jensen, R. E. Palmer, W. Allison, and J. F. Annett, Phys. Rev. Lett. **66**, 492 (1991).

[58] L. D. Landau, *Collected Papers* (Gordon and Breach, New York, 1965), pp. 67–68.

[59] F. Gervais, J.-L. Servoin, A. Baratoff, J. G. Bednorz, and G. Binnig, Phys. Rev. B **47**, 8187 (1993).

[60] D. M. Eagles, M. Georgiev, and P. C. Petrova, Phys. Rev. B **54**, 22 (1996).

[61] C. Bi, J. Ma, J. Yan, X. Fang, B. Zhao, D. Yao, and X. Qiu, J. Phys.: Condens. Matter **18**, 2553 (2006).

[62] Y. Zhou and A. J. Millis, Phys. Rev. B **93**, 224506 (2016).

[63] H. Zhang, D. Zhang, X. Lu, C. Liu, G. Zhou, X. Ma, L. Wang, P. Jiang, Q.-K. Xue, and X. Bao, Nat. Commun. **8**, 214 (2017).

[64] C. Liu, J. Mao, H. Ding, R. Wu, C. Tang, F. Li, K. He, W. Li, C.-L. Song, X.-C. Ma, Z. Liu, L. Wang, and Q.-K. Xue, Phys. Rev. B **97**, 024502 (2018).